Sex-specific pathophysiological mGluR5-dependent Aβ oligomer signaling in Alzheimer mice

Khaled S. Abd-Elrahman[1,2,3#], Alison Hamilton[1,2,#], Jessica M. de Souza[1,2,4], Awatif Albaker[1,2], Fabiola M. Ribeiro[4] and Stephen S. G. Ferguson[1,2,*]

University of Ottawa Brain and Mind Institute[1], Department of Cellular and Molecular Medicine[2], University of Ottawa, 451 Smyth Road, Ottawa, Ontario, K1H 8M5, Canada.

Department of Pharmacology and Toxicology[3], Faculty of Pharmacy, Alexandria University, Alexandria, 21521, Egypt.

Department of Biochemistry and Immunology[4], ICB, Universidade Federalde Minas Gerais, Belo Horizonte, Brazil.

[#]Co-first authors

*Address correspondence to:

Dr. Stephen S. G. Ferguson

Department of Cellular and Molecular Medicine, University of Ottawa,

451 Smyth Dr. Ottawa, Ontario, Canada, K1H 8M5. Tel: (613) 562 5800 Ext 8889.
sferguso@uottawa.ca

ABSTRACT

Sex is an important modifier of Alzheimer's disease (AD) prevalence and progression. Aβ oligomers engage metabotropic glutamate receptor 5 (mGluR5) to mediate pathological signaling in AD. We find here, that mGluR5 signaling is intrinsically different in male versus female mouse neurons, as mGluR5 agonist and Aβ oligomer treatments inactivate a GSK3β/ZBTB16/ATG14-regulated autophagy pathway via Ser9 phosphorylation of GSK3β in an mGluR5-dependent mechanism in male, but not female, primary neuronal cultures. These observed sex-specific differences in mGluR5 signaling translate into *in vivo* differences in mGluR5-dependent pathological signaling in male and female AD mice. We demonstrate that treatment of male, but not female, APPswe/PS1ΔE9 mice with the mGluR5-selective negative allosteric modulator (NAM), CTEP, improved cognition, reduced Aβ oligomer-mediated pathology, attenuated inflammatory responses and enhanced autophagy in only male APPswe/PS1ΔE9 mice. These differences in male versus female APPswe/PS1ΔE9 responses to CTEP correlate with sex-specific differences in cell surface mGluR5 trafficking. This study demonstrates clear sex-specific differences in mGluR5 cellular signaling and trafficking in a mouse model of AD and strongly indicates a need to redesign and reanalyze sex-specific AD treatment strategies.

SHORT RUNNING TITLE: Sex-specific Aβ signaling in Alzheimer's disease

KEY WORDS Alzheimer's disease, autophagy, cognition, mGluR5, neuroglia, sex

Introduction

Alzheimer's disease (AD) is a progressive neurodegenerative disease that is characterized by age-related memory loss and cognitive decline. It is the most prevalent cause of dementia, accounting for ~60–80% of diagnosed dementia cases (*1*, *2*). Despite this alarming prevalence, there are currently no available treatments capable of modifying or reversing the progression of AD (*3*, *4*). The etiology of AD remains to be fully elucidated, although two proteins are considered the pathological hallmarks of AD that primarily contribute to the neurotoxicity associated with the disease. These proteins, β-amyloid (Aβ) oligomers and hyper-phosphorylated tau protein, accumulate as the disease progresses causing disruption in neuronal signaling and neurodegeneration (*5*–*8*).

There is growing evidence to suggest that sex is an important modulator of AD prevalence and progression with clinical and preclinical studies demonstrating that the incidence of developing AD is higher in females than for age- and risk factor-matched males (*9*–*12*). The higher incidence of cognitive impairment in women compared to men at the same stage of AD has been long attributed to reduced estrogen and/or estrogen receptors levels following menopause, since estrogen has been linked experimentally to numerous neuroprotective actions relevant to cognitive function in animal models of disease (*13*–*15*). However, the first large-scale clinical study (Women's Health Initiative Memory Study, WHIMS) demonstrated an increased risk of dementia and poor cognitive outcomes in postmenopausal women randomized to hormone-replacement therapy, thereby removing clinical support for this hypothesis (*16*, *17*).

Glutamate, the main excitatory brain neurotransmitter, plays a key role in learning and memory and the Gq-coupled metabotropic glutamate receptors, subtype 5 (mGluR5) is of a particular interest in AD pathology (*18*, *19*). Metabotropic glutamate receptor 5 (mGluR5) is of particular interest in AD pathology, as it acts as an extracellular scaffold for Aβ oligomers to

promote mGluR5 clustering, increase intracellular Ca^{2+} release and inhibit autophagy, all of which contribute to the synaptic dysfunction and neurotoxicity associated with cognitive dysfunction (*20*–*24*). We and others have demonstrated that both pharmacological and genetic silencing of mGluR5 reverses cognitive deficits and reduces Aβ pathology in both APPswe/PS1ΔE9 and 3xTg-AD male mouse models of AD (*20*–*25*). While these studies emphasized the key role of mGluR5 in AD pathophysiology in male mouse models of AD, it is not yet clear whether alterations in mGluR5 signaling is conserved between male and female AD mice.

Given that both clinical and experimental evidence indicate a divergent AD pathology between males and female, the dramatic drug treatment failure rate in AD clinical trials warrant a better delineation of the molecular signaling mechanism(s) underlying sex-related pathophysiological differences in AD (*9*, *11*). In the present study, we find that either mGluR5 agonist or Aβ oligomer treatment results in the phosphorylation of GSK3β at Ser9 and inhibition of the GSK3/ZBTB16/ATG14-regulated autophagy pathway in primary cortical neurons derived from male, but not female wild-type E18 embryos. This observed sex-specific regulation of mGluR5 signaling by Aβ oligomers translates *in vivo* where the mGluR5-selective negative allosteric modulator (NAM), CTEP, improved cognition, reduced Aβ oligomer-mediated pathology, attenuated inflammatory responses and enhanced autophagy in only male APPswe/PS1ΔE9 mice. These studies have important implications regarding the successful repurposing of mGluR5 NAMs for the treatment of neurodegenerative disease. Moreover, they suggest the need for the sex-specific stratification of neurodegenerative drug trial results that will impact the guidance of future design of sex-specific treatment strategies.

RESULTS

Sex-specific mGluR5-dependent inactivation of a GSK3β/ZBTB16-autophagic pathway in primary neuronal cultures

Aβ oligomer activation of mGluR5 has been associated with impaired cognition, Aβ pathology and the inhibition of a GSK3β/ZBTB16/ATG14 autophagy pathway in male APPswe/PS1ΔE9 mice (*20*, *23*, *24*). To test possible sex-specific differences in agonist and Aβ oligomer-dependent antagonism of autophagy following mGluR5 activation, we treated cultured male and female cortical (14 DIV) neurons with either DHPG (100 μM) or $Aβ_{1-42}$ oligomers (100 nM) in the presence or absence of the mGluR5 selective NAM, CTEP (2-chloro-4-[2[2,5-dimethyl-1-[4-(trifluoromethoxy) phenyl] imidazol-4-yl] ethynyl] pyridine) (10 μM). DHPG and $Aβ_{1-42}$ oligomers induced GSK3β phosphorylation and inhibited autophagy, as measured by an increase in p62 expression in male, but not in female, neuronal cultures in a manner that is inhibited by CTEP (Fig. 1A and B). Interestingly, only $Aβ_{1-42}$ oligomers increased ZBTB16 expression solely in male cultures (Fig. 1A and B), which suggested that $Aβ_{1-42}$ can be potent inhibitor of autophagy as previously reported (*24*, *26*) . These observations suggested that there are unexpected important sex-specific differences in mGluR5 signaling in response to extra-neuronal Aβ oligomers.

mGluR5 blockade improves cognitive deficits in male, but not female, APPswe/PS1ΔE9 mice

We then sought to determine whether sex-specific differences in mGluR5 signaling *in vitro* translated into sex-specific differences in the mechanism by which Aβ oligomers mediate cognitive dysfunction and Aβ deposition *in vivo*. To test this, 9-month-old male and female wild-type and APPswe/PS1ΔE9 mice were tested for impairments in working and spatial memory in the novel object recognition, Morris water maze (MWM) and Morris water maze with reversal (RMWM) task following treatment with CTEP (2 mg/Kg for 12 weeks). This treatment regime

previous improved cognitive deficits in 12-month-old male APPswe/PS1ΔE9 and 3xTg mice that were treated for 12 weeks with CTEP (*23*, *27*, *28*). We found that vehicle-treated 9-month-old wild-type male and female mice discriminated between novel and familiar objects, whereas 9-month-old vehicle-treated male and female APPswe/PS1ΔE9 mice were not able to discriminate between familiar and novel objects (Fig. 2A and 2B). After chronic treatment (12 weeks) with CTEP, 9-month-old male APPswe/PS1ΔE9 mice regained the capacity to discriminate between the objects, whereas female APPswe/PS1ΔE9 mice remained cognitively-impaired (Fig. 2A and 2B). Discrepancies in cognitive function between males and females following CTEP treatment could not be attributed to difference in either object place preference, locomotor or exploratory behavior between both sexes (Fig. 2C and 2D and Fig. S1). Subsequently, mice from each experimental group were tested in the MWM and RMWM. We found that vehicle-treated male and female APPswe/PS1ΔE9 mice exhibited significantly longer escape latencies, greater path lengths and less time spent in target quadrant than did similarly treated same sex wild-type mice in the MWM (Fig.3A-D). However, CTEP treatment improved male APPswe/PS1ΔE9 mouse performance in the MWM, as measured by shorter escape latency, path lengths and longer time spent in target quadrant with values indistinguishable from wild-type (Fig. 3A-D). In contrast, CTEP treatment did not improve either escape latency, path length, swim speed or time spent in target quadrant for female APPswe/PS1ΔE9 mice in the MWM, when compared to vehicle-treated APPswe/PS1ΔE9 female mice (Fig. 3A-D). Results from the RMWM were similar to the MWM showing a rescue in spatial memory deficits in male, but not female, APPswe/PS1ΔE9 mice following treatment with CTEP (Fig. 3E-H). CTEP treatment of female, but not male, wild-type mice was associated with a longer escape latency, longer path length, slower swim speed and shorter time spent in target quadrant compared to vehicle-treated female mice, an observation not evident in male counterparts (Fig. 3E-H). Taken together, both male and female APPswe/PS1ΔE9 mice presented with a similarly impaired cognitive phenotype, but mGluR5

antagonism only improved working and spatial memory in male mice indicating a potential sex-specific regulation of mGluR5-mediated pathology in APPswe/PS1ΔE9 mice.

mGluR5 inhibition reduces Aβ oligomers and plaques in male, but not female, APPswe/PS1ΔE9 mice via a ZBTB16/ATG14-regulated autophagy pathway

To test whether the sex-specific improvement in cognitive function following mGluR5 inhibition was paralleled by similar changes in Aβ pathology we examined whether Aβ plaque density was reduced following CTEP treatment in coronal slices of male and female APPswe/PS1ΔE9 cortex and hippocampus. We found that the deposition of Aβ plaque density was significantly reduced in male, but not female, APPswe/PS1ΔE9 cortical and hippocampal brain slices following CTEP treatment (Fig. 4A and 4B). We then assessed Aβ oligomer levels in vehicle- and CTEP-treated male and female APPswe/PS1ΔE9 mouse lysates. We detected a comparable increase in soluble Aβ oligomers level in both male and female APPswe/PS1ΔE9 mice versus age- and sex-matched wild-type mice (Fig. 4C). The elevated levels of Aβ oligomers detected in male APPswe/PS1ΔE9 brain lysates were significantly reduced following treatment with CTEP, but Aβ oligomer concentrations remained elevated in CTEP-treated female APPswe/PS1ΔE9 mice (Fig. 4C). These observations indicated that pharmacological blockade of mGluR5 had a positive outcome in male APPswe/PS1ΔE9 mice, while having a negative outcome in female APPswe/PS1ΔE9 mice.

Previously, we demonstrated that clearance of Aβ and huntingtin pathological species was increased by inhibiting Aβ oligomer/mutant huntingtin-stimulated pathological activation of mGluR5 that resulted in the inhibition of a novel GSK3β/ZBTB16/ATG14 autophagy pathway in male mice (*24*, *29*). We found here that GSK3β-pS9 phosphorylation was significantly increased in brain lysates of vehicle-treated APPswe/PS1ΔE9 male mice and that CTEP significantly reduced GSK3β phosphorylation leading to its activation. (Fig. 4D). This resulted in decreased

protein expression levels of the ubiquitin ligase ZBTB16 and consequently increased expression of ATG14 which facilitated autophagy, as evidenced by a significant reduction in the protein expression level of the autophagy marker p62 in male APPswe/PS1ΔE9 male mice (Fig. 4D-G). Interestingly, we detected no change in GSK3β phosphorylation and either ZBTB16 or ATG14 expression in female APPswe/PS1ΔE9 mice (Fig. 4D-F). We also detected an unexplainable elevation in P62 expression in vehicle- and CTEP-treated wild-type and APPswe/PS1ΔE9 female mice when compared to vehicle-treated wild-type male mice (Fig. 4G). Taken together, our results show that while defects in autophagy may contribute to AD-like neuropathology in both sexes of APPswe/PS1ΔE9 mice, the contribution of ZBTB16- autophagic pathway to Aβ pathology was exclusive to male mice.

mGluR5 inhibition reduces neuroglial activation and promotes neuronal and synaptic recovery in male, but not female, APPswe/PS1ΔE9 mice

The neuroinflammatory response triggered by glial cells, astrocytes and microglia, contribute synaptic dysfunction and neuronal death in AD (*30*–*32*) , a response that was blunted in male APPswe/PS1ΔE9 following CTEP treatment . Specifically, microglia (Iba1 positive cells) and astrocytes (GFAP positive cells) were previously detected around Aβ plaques (*30*–*33*). We found that the number of Iba1- and GFAP-positive cells were significantly elevated to a similar level in cortical brain slices of both male and female APPswe/PS1ΔE9 mice (Fig. 5A and 5B). CTEP treatment reduced the markers of activated microglia and reactive astrocytes in male, but not female APPswe/PS1ΔE9 brain slices (Fig 5A and 5B). We also detected a significant reduction in the number of NeuN positive neurons in vehicle-treated APPswe/PS1ΔE9 female mice that was not affected by CTEP treatment, whereas no loss of NeuN staining was observed in male APPswe/PS1ΔE9 mice (Fig. 5C). We also observe synapse reduction in both male and female APPswe/PS1ΔE9 mice, but CTEP treatment of male mice only prevented synaptic loss (Fig. 5D).

Sex-specific differences in the cell surface trafficking of mGluR5 in male and female APPswe/PS1ΔE9 mice

Our neuronal cell culture experiments indicated mGluR5 signaling was intrinsically different in male and female neurons. However, this did not necessarily account for effects of Aβ oligomer signaling and mGluR5 regulation in adult male and female APPswe/PS1ΔE9 mice. Since Aβ oligomers could activate and promote mGluR5 clustering at synapses to exacerbate AD pathology (*20–22*), it was possible that mGluR5 was differentially-expressed in males and females leading to the discordant sex-specific contribution of mGluR5 to AD pathogenesis. Therefore, we examined whether the total and/or cell surface expression of mGluR5 was different between male and female APPswe/PS1ΔE9 mice, when compared to wild-type controls. Coronal brain slices from hippocampus and cortex of 6-month-old mice were used to determine total mGluR5 expression, as well as the plasma membrane expression for mGluR5 by performing a cell surface protein biotinylation. As we have previously reported (*23–25*), no change in total expression of mGluR5 was detected in male APPswe/PS1ΔE9 mice, but cell surface expression of mGluR5 was increased in hippocampus and cortex of male APPswe/PS1ΔE9 mice relative to wild-type mice (Fig. 6A and 6B). Surprisingly, the cell surface expression of mGluR5 was nearly abolished in both the hippocampus and cortex of female APPswe/PS1ΔE9 mice relative to wild-type mice (Fig 6A). However, total cellular mGluR5 expression in both the cortex and hippocampus was not different between male and female APPswe/PS1ΔE9 mice when compared to age- and sex-matched wild-type male and female mice at 6 months of age (Fig. 6B). The observed change in mGluR5 surface expression in male and female APPswe/PS1ΔE9 mice was also detected in mice as early as 2 months of age (Fig. S2).

DISCUSSION

One major challenge in AD therapy is the identification of a pharmaceutical target that does not only manage disease symptomology, but also modifies disease progression. Genetic silencing has clearly demonstrated a contributory role of mGluR5 in AD pathogenesis, specifically Aβ-related pathology in male APPswe/PS1ΔE9 mice (*25*). Furthermore, while both negative and silent mGluR5 modulators rescue AD mouse behavioral phenotypes, only mGluR5 NAMs treatment mitigated Aβ pathology in a preclinical male APPswe/PS1ΔE9 and 3xTg-AD mouse models of AD (*20*, *23*, *34*). However, gender-specific responses to therapies have been reported in many neurological diseases including AD that further complicated the process of drug discovery (*9–11*). We find that neuronal cultures from male and female mouse embryos manifest with sex-specific responses to Aβ-mediated activation of mGluR5. Specifically, Aβ oligomer treatment of wild-type female neurons in culture does not elicit GSK3β phosphorylation resulting in the inhibition of the GSK3β/ZBTB16/ATG14-regulated autophagy pathway. We also demonstrate that the contribution of mGluR5 to AD-like neuropathology and response to mGluR5 NAM treatment *in vivo* is different between male and female APPswe/PS1ΔE9 despite similar degrees of cognitive impairment, neuroinflammation and Aβ-related pathology. Moreover, mGluR5 surface expression in male APPswe/PS1ΔE9 mice is increased and is associated with the mGluR5-dependent inhibition of a ZBTB16-mediated autophagy mechanism, accumulation of Aβ oligomers and plaques and exacerbated neuroinflammation. Treatment with an mGluR5 NAM corrected mGluR5 signaling, reduced neuroglial activation, initiated autophagy and improved in Aβ pathology and cognitive functions in male APPswe/PS1ΔE9 mice. In contrast, female APPswe/PS1ΔE9 exhibit diminished cell surface expression of mGluR5, which is not associated with mGluR5-dependent inhibition of signaling via the ZBTB16-mediated autophagy pathway. This results in the inability of CTEP to mitigate cognitive impairment, the accumulation of Aβ oligomers and plaques, as well as reduce neuroinflammation. Thus, it is evident that mGluR5

contribution to the etiology and treatment of AD neuropathology is sex-dependent. This raises the distinct possibility that there are fundamentally important sex-dependent differences in the mechanisms underlying the cellular regulation of mGluR5 signaling.

Novel object recognition and Morris water maze tasks reveal a significant impairment in both working and spatial memory in both vehicle-treated 9-month-old male and female APPswe/PS1ΔE9 mice. Moreover, the deposition of Aβ plaques and levels of soluble Aβ oligomers in the hippocampus and cortex of APPswe/PS1ΔE9 from both sexes exhibit similar increases. Thus, our pathological and behavioral findings in APPswe/PS1ΔE9 mice are consistent with published reports showing a progressive Aβ deposition and cognitive impairment starting at 6 months of age and robust accumulation of plaques by 9 months (*31*, *35*). However, the inhibition of mGluR5 significantly reverses cognitive deficits and reduces Aβ deposition in only male, but not female, APPswe/PS1ΔE9 mice. Our study suggests that mGluR5 NAM treatment can be effectively repurposed at an earlier disease stage in male APPswe/PS1ΔE9 mice to effectively reverse cognitive impairment and improve Aβ-related pathology, but that this pharmacological treatment will be ineffective in female mice. To our knowledge this study represents the first evidence that mGluR5 is not a central contributor to AD-related neuropathology in female AD mice.

Aβ oligomers are a normal proteolytic byproduct of the metabolism of amyloid precursor protein (APP) and is normally found as a soluble protein at low levels in the brain. However, alterations in the production and/or clearance of Aβ oligomers can shift the homeostasis towards increased $A\beta_{1\text{-}42}$ levels and be detrimental resulting in accelerated neurodegeneration (*5*, *6*). Therefore, enormous effort has been put forward to identify the pathways that regulate Aβ accumulation. Within this context, autophagy is an interesting target as an essential degradation pathway and defects in autophagy have been implicated in several proteinopathies including AD (*36*–*39*). Indeed, evidence suggests that autophagy deficits occur in the early stages of AD both

animal models and patients (*26*, *37*, *40*). We have demonstrated that mGluR5 inhibits autophagy through a ZBTB16-Cullin3-Roc1 E3-ubiquitin ligase pathway in male APPswe/PS1ΔE9 and 3xTg-AD mouse models (*24*, *41*). In the current study, we find that treatment with mGluR5 NAM results in a GSK3β-dependent increase in ATG14 and activated autophagy in male APPswe/PS1ΔE9 mice, but we observe no increases in GSK3β phosphorylation or ATG14 expression in vehicle-treated female APPswe/PS1ΔE9 mice when compared with either male or female wild-type mice. While the pharmacological inhibition of mGluR5 leads to the activation of the GSK3β/ZBTB16/ATG14-regulated autophagy pathway and is key for the removal of Aβ oligomer load in males APPswe/PS1ΔE9 mice, mGluR5 does not appear to be engaged in negatively regulating this pathway in female APPswe/PS1ΔE9 mice. This may explain, at least in part, why the mGluR5 NAM tested in this study is effective in reducing Aβ oligomers/plaques and improving cognitive function in male APPswe/PS1ΔE9 mice only.

Aβ oligomers stimulate microglia leading to the release of inflammatory mediators that exacerbate the neuronal inflammatory burden (*30*, *31*, *42*, *43*). Astrocytes also serve as a constant and important source of neurotrophic factors such as BDNF under physiological conditions that can be also activated by Aβ oligomers to generate reactive oxygen species, release glutamate and block glutamate reuptake that are associated with neurotoxicity and neuronal death in AD (*44*–*47*). We find that makers of microglia activation and astrogliosis, Iba1 and GFAP, respectively, are significantly increased in 9-month-old male and female APPswe/PS1ΔE9 brain slices. This is consistent with previous findings showing that markers of activated microglia and reactive astrocytes can be detected as early as 6-month-old APPswe/PS1ΔE9 mice around Aβ plaques (*31*, *43*). mGluR5 blockade reduces Iba1 and GFAP in male APPswe/PS1ΔE9 mice yet is ineffective in females. Thus, it is possible that the autophagic clearance of Aβ oligomers following treatment with mGluR5 NAM in male APPswe/PS1ΔE9 mice reduces Aβ oligomer-activated neurogliosis resulting in the blockade of neurotoxicity caused by glutamate overspill from astrocyte.

Our findings clearly indicate that both male and female APPswe/PS1ΔE9 mice present with a comparable cognitive impairment and Aβ oligomer burden, but are associated with clearly divergent effects on the regulation of mGluR5-mediated signaling. Thus, we examined whether mGluR5 cell surface expression differs between the sexes and whether this might contribute to observed differences in downstream mGluR5 signaling in male and female APPswe/PS1ΔE9 mice. We find that mGluR5 surface expression is upregulated in male APPswe/PS1ΔE9 mice, while cell surface mGluR5 expression is almost completely abolished in female APPswe/PS1ΔE9 mice. Since we know that Aβ oligomers can activate and promote mGluR5 clustering at synapses to exacerbate AD pathology (*20–22*), this increased delivery of mGluR5 to cell surface in male APPswe/PS1ΔE9 mice will further enhance the accessibility for activation and clustering by Aβ oligomers and accelerate glutamatergic excitotoxicity. CTEP, along with its ability to activate autophagic clearance of Aβ oligomers, may also function to disrupt the interaction between Aβ oligomers and mGluR5 via binding to the allosteric site of mGluR5 and consequently slow Aβ oligomer-mediated neurodegenerative mechanisms in male mice. Conversely, in female APPswe/PS1ΔE9 the delivery of mGluR5 to cell surface is impaired, despite similar total mGluR5 expression in wild-type animals of both sexes. Thus, it seems that mGluR5 contribution to the neurodegenerative process in female AD mice is minimal and this can explain why mGluR5 NAM is not effective in mitigating AD-like symptoms or pathology in females. Moreover, mGluR5 signaling in response to agonist or Aβ oligomer treatment was not engaged in wild-type female neuronal cultures suggesting that there may be fundamental differences in the normal engagement of mGluR5 signaling in male and female brain tissue.

In summary, we find that mGluR5 antagonism is effective in reducing cognitive impairments, pathological hallmarks, neuroinflammation and cell death associated with AD only in male AD mice. Thus, we provide robust evidence that aspects of mGluR5 signaling and function are not conserved between APPswe/PS1ΔE9 male and female mice and there are sex-

specific differences that must be considered when embracing mGluR5 as a potential drug target for AD in females and potentially other diseases. Consequently, enhanced effort needs to be directed toward exploiting novel targets in females to effectively slow the neurodegenerative process and ameliorate the progression of AD-related cognitive deficits.

REFERENCES

1. J. K. Y. Yap, B. S. Pickard, E. W. L. Chan, S. Y. Gan, The Role of Neuronal NLRP1 Inflammasome in Alzheimer's Disease: Bringing Neurons into the Neuroinflammation Game. *Mol. Neurobiol.*, 1–13 (2019).

2. L. Rizzi, I. Rosset, M. Roriz-Cruz, Global Epidemiology of Dementia: Alzheimer's and Vascular Types. *Biomed Res. Int.* **2014**, 1–8 (2014).

3. D. A. Casey, D. Antimisiaris, J. O'Brien, Drugs for Alzheimer's disease: are they effective? *P T*. **35**, 208–11 (2010).

4. K. L. Lanctôt, R. D. Rajaram, N. Herrmann, Therapy for Alzheimer's Disease: How Effective are Current Treatments? *Ther. Adv. Neurol. Disord.* **2**, 163–80 (2009).

5. S. Hunter, C. Brayne, Understanding the roles of mutations in the amyloid precursor protein in Alzheimer disease. *Mol. Psychiatry* (2017), doi:10.1038/mp.2017.218.

6. F. Kamenetz *et al.*, APP processing and synaptic function. *Neuron*. **37**, 925–37 (2003).

7. A. Hamilton, G. W. Zamponi, S. S. G. Ferguson, Glutamate receptors function as scaffolds for the regulation of β-amyloid and cellular prion protein signaling complexes. *Mol. Brain*. **8**, 18 (2015).

8. J. C. Polanco *et al.*, Amyloid-β and tau complexity — towards improved biomarkers and targeted therapies. *Nat. Rev. Neurol.* **14**, 22–39 (2017).

9. J. L. Podcasy, C. N. Epperson, Considering sex and gender in Alzheimer disease and other dementias. *Dialogues Clin. Neurosci.* **18**, 437–446 (2016).

10. D. W. Fisher, D. A. Bennett, H. Dong, Sexual dimorphism in predisposition to Alzheimer's disease. *Neurobiol. Aging*. **70**, 308–324 (2018).

11. H. Hampel *et al.*, Precision medicine and drug development in Alzheimer's disease: the importance of sexual dimorphism and patient stratification. *Front. Neuroendocrinol.* **50**, 31–51 (2018).

12. R. S. Vest, C. J. Pike, Gender, sex steroid hormones, and Alzheimer's disease. *Horm. Behav.* **63**, 301–307 (2013).

13. K. R. Laws, K. Irvine, T. M. Gale, Sex differences in cognitive impairment in Alzheimer's disease. *World J. Psychiatry*. **6**, 54 (2016).

14. Y. Tang *et al.*, Estrogen-related receptor alpha is involved in Alzheimer's disease-like pathology. *Exp. Neurol.* **305**, 89–96 (2018).

15. J. F. Kelly *et al.*, Levels of estrogen receptors alpha and beta in frontal cortex of patients with Alzheimer's disease: relationship to Mini-Mental State Examination scores. *Curr. Alzheimer Res.* **5**, 45–51 (2008).

16. S. R. Rapp *et al.*, Effect of estrogen plus progestin on global cognitive function in postmenopausal women: the Women's Health Initiative Memory Study: a randomized controlled trial. *JAMA*. **289**, 2663–72 (2003).

17. A. C. McCarrey, S. M. Resnick, Postmenopausal hormone therapy and cognition. *Horm. Behav.* **74**, 167–172 (2015).

18. F. M. Ribeiro, L. B. Vieira, R. G. W. Pires, R. P. Olmo, S. S. G. Ferguson, Metabotropic glutamate receptors and neurodegenerative diseases. *Pharmacol. Res.* **115**, 179–191 (2017).

19. C. M. Niswender, P. J. Conn, Metabotropic Glutamate Receptors: Physiology, Pharmacology, and Disease. *Annu. Rev. Pharmacol. Toxicol.* **50**, 295–322 (2010).

20. J. W. Um *et al.*, Metabotropic Glutamate Receptor 5 Is a Coreceptor for Alzheimer Aβ Oligomer Bound to Cellular Prion Protein. *Neuron*. **79**, 887–902 (2013).

21. M. Renner *et al.*, Deleterious effects of amyloid beta oligomers acting as an extracellular scaffold for mGluR5. *Neuron*. **66**, 739–54 (2010).

22. D. K. Sokol, B. Maloney, J. M. Long, B. Ray, D. K. Lahiri, Autism, Alzheimer disease, and fragile X: APP, FMRP, and mGluR5 are molecular links. *Neurology*. **76**, 1344–52 (2011).

23. A. Hamilton *et al.*, Chronic Pharmacological mGluR5 Inhibition Prevents Cognitive Impairment and Reduces Pathogenesis in an Alzheimer Disease Mouse Model. *Cell Rep.* **15**, 1859–65 (2016).

24. K. S. Abd-Elrahman, A. Hamilton, M. Vasefi, S. S. G. Ferguson, Autophagy is increased following either pharmacological or genetic silencing of mGluR5 signaling in Alzheimer's disease mouse models. *Mol. Brain*. **11** (2018), doi:10.1186/s13041-018-0364-9.

25. A. Hamilton, J. L. Esseltine, R. A. DeVries, S. P. Cregan, S. S. G. Ferguson, Metabotropic glutamate receptor 5 knockout reduces cognitive impairment and pathogenesis in a mouse model of Alzheimer's disease. *Mol. Brain*. **7**, 40 (2014).

26. Q. Li, Y. Liu, M. Sun, Autophagy and Alzheimer's Disease. *Cell. Mol. Neurobiol.* **37**, 377–388 (2017).

27. L. Lindemann *et al.*, CTEP: a novel, potent, long-acting, and orally bioavailable metabotropic glutamate receptor 5 inhibitor. *J. Pharmacol. Exp. Ther.* **339**, 474–86 (2011).

28. G. Jaeschke *et al.*, Metabotropic Glutamate Receptor 5 Negative Allosteric Modulators: Discovery of 2-Chloro-4-[1-(4-fluorophenyl)-2,5-dimethyl-1 *H* -imidazol-4-ylethynyl]pyridine (Basimglurant, RO4917523), a Promising Novel Medicine for Psychiatric Diseases. *J. Med. Chem.* **58**, 1358–1371 (2015).

29. K. S. Abd-Elrahman *et al.*, mGluR5 antagonism increases autophagy and prevents disease progression in the *zQ175* mouse model of Huntington's disease. *Sci. Signal.* **10**, eaan6387 (2017).

30. H. Chun, I. Marriott, C. J. Lee, H. Cho, Elucidating the Interactive Roles of Glia in Alzheimer's Disease Using Established and Newly Developed Experimental Models. *Front. Neurol.* **9**, 797 (2018).

31. L. Ruan, Z. Kang, G. Pei, Y. Le, Amyloid deposition and inflammation in APPswe/PS1dE9 mouse model of Alzheimer's disease. *Curr. Alzheimer Res.* **6**, 531–40 (2009).

32. W. Kamphuis, M. Orre, L. Kooijman, M. Dahmen, E. M. Hol, Differential cell proliferation in the cortex of the appsweps1de9 alzheimer's disease mouse model. *Glia*. **60**, 615–629 (2012).

33. R. Luo *et al.*, Activation of PPARA-mediated autophagy reduces Alzheimer disease-like pathology and cognitive decline in a murine model. *Autophagy*, 1–18 (2019).

34. L. T. Haas *et al.*, Silent Allosteric Modulation of mGluR5 Maintains Glutamate Signaling while Rescuing Alzheimer's Mouse Phenotypes. *Cell Rep.* **20**, 76–88 (2017).

35. J. L. Jankowsky *et al.*, Mutant presenilins specifically elevate the levels of the 42 residue beta-amyloid peptide in vivo: evidence for augmentation of a 42-specific gamma secretase. *Hum. Mol. Genet.* **13**, 159–70 (2004).

36. S. Sarkar, D. C. Rubinsztein, Small molecule enhancers of autophagy for neurodegenerative diseases. *Mol. Biosyst.* **4**, 895–901 (2008).

37. D. C. Rubinsztein *et al.*, Autophagy and its possible roles in nervous system diseases, damage and repair. *Autophagy*. **1**, 11–22 (2005).

38. J. Nah, J. Yuan, Y.-K. Jung, Autophagy in neurodegenerative diseases: from mechanism to therapeutic approach. *Mol. Cells*. **38**, 381–9 (2015).

39. R. A. Nixon, The role of autophagy in neurodegenerative disease. *Nat. Med.* **19**, 983–997 (2013).

40. M. E. Orr, S. Oddo, Autophagic/lysosomal dysfunction in Alzheimer's disease. *Alzheimers. Res. Ther.* **5**, 53 (2013).

41. T. Zhang *et al.*, G-protein-coupled receptors regulate autophagy by ZBTB16-mediated ubiquitination and proteasomal degradation of Atg14L. *Elife*. **4**, e06734 (2015).

42. P. L. McGeer, E. G. McGeer, The inflammatory response system of brain: implications for therapy of Alzheimer and other neurodegenerative diseases. *Brain Res. Brain Res. Rev.* **21**, 195–218 (1995).

43. W. Kamphuis *et al.*, GFAP isoforms in adult mouse brain with a focus on neurogenic astrocytes and reactive astrogliosis in mouse models of Alzheimer disease. *PLoS One*. **7**, e42823 (2012).

44. A. Y. Abramov, -Amyloid Peptides Induce Mitochondrial Dysfunction and Oxidative Stress in Astrocytes and Death of Neurons through Activation of NADPH Oxidase. *J. Neurosci.* **24**, 565–575 (2004).

45. J. J. Rodríguez, M. Olabarria, A. Chvatal, A. Verkhratsky, Astroglia in dementia and Alzheimer's disease. *Cell Death Differ.* **16**, 378–85 (2009).

46. M. Matos, E. Augusto, C. R. Oliveira, P. Agostinho, Amyloid-beta peptide decreases glutamate uptake in cultured astrocytes: involvement of oxidative stress and mitogen-activated protein kinase cascades. *Neuroscience*. **156**, 898–910 (2008).

47. O. Pascual, S. Ben Achour, P. Rostaing, A. Triller, A. Bessis, Microglia activation triggers astrocyte-mediated modulation of excitatory neurotransmission. *Proc. Natl. Acad. Sci. U. S. A.* **109**, E197-205 (2012).

48. S. J. Tunster, Genetic sex determination of mice by simplex PCR. *Biol. Sex Differ.* **8**, 31 (2017).

ACKNOWLEDGMENTS

S.S.G.F is a Tier I Canada Research Chair in Brain and Mind. K.S.A is a Lecturer in the Department of Pharmacology & Toxicology, Faculty of Pharmacy, Alexandria University, Egypt. Thanks to Shaunessy Hutchinson for breeding the colony and to the behavior core at the University of Ottawa.

FUNDING

This study was supported by grants from Canadian Institutes for Health Research (CIHR) PJT-148656 and PJT-165967 to S.S.G.F, and clinician postdoctoral fellowship from the Alberta Innovates Health Solutions (AIHS) and CIHR to K.S.A.

AUTHOR CONTRIBUTIONS

K.S.A., A.H., F.M.R. and S.S.G.F were responsible for the conception and design of all experiments. K.S.A., A.H., A. A. and J.M.D. performed the experiments and analyzed the data. K.S.A and S.S.G.F wrote the manuscript. S.S.G.F supervised the study.

COMPETING INTERETS: Authors declare no competing interests.

DATA AND MATERIAL AVILABILITY: All data is available in the main text or the Supplementary materials

MATERIALS AND METHODS

Reagents: CTEP was purchased from Axon Medchem (1972). Horseradish peroxidase (HRP)-conjugated anti-rabbit IgG secondary antibody was from Bio-Rad. HRP-conjugated anti-mouse secondary and rabbit GSK3β (pS9, 9323), mouse anti-GSK3β (9832) antibodies were from New England Biolabs. Rabbit anti-actin (CL2810AP) and ATG14L (PD026) were from Cedarlane. Mouse anti-P62 (56416) and rabbit anti-ZBTB16 (39354), -Synaptophysin (14692), -GFAP (7260), -vinculin (129002) and -Iba1 (178847) antibodies were from Abcam. Rabbit anti-mGluR5 (AB5675) and mouse Anti-NeuN (MAB377) from Sigma-Aldrich. Rabbit anti-β-Amyloid (715800), Donkey anti-mouse Alexa Fluor 647 (A31571) and goat anti-mouse 488 (A11001) were from Thermo Scientific. Reagents used for western blotting were purchased from Bio-Rad and all other biochemical reagents were from Sigma-Aldrich.

Animals: STOCK B6C3-Tg (APPswe/PSEN1ΔE9)85Dbo/J mice (APPswe) that carry the human APP with Swedish mutation and the DeltaE9 mutation of the human presenilin 1 gene (*35*) were purchased from Jackson Laboratory (Bar Harbor, ME). Offspring were tail snipped and genotyped using PCR with primers specific for the APP sequence. Animals were bred to establish littermate controlled female and male wild-type (WT), group-housed in cages of 2 or more animals, received food and water *ad libitum* and maintained on a 12-hour light/12hour dark cycle at 24°C. Groups of 24 male and female wild-type and APPswe/PS1ΔE9 mice were aged to 6 months of age and 12 mice from each group were treated every 48h with either vehicle (DMSO in chocolate pudding) or CTEP (2 mg/kg, dissolved in 10% DMSO then mixed with chocolate pudding, final DMSO concentration was 0.1%) for 12 weeks (*23*, *29*). The drug dose was calculated weekly based on weight. Cognitive and locomotor functions of all animals were assessed prior to and following 12 weeks of drug treatment. At the end of the 12-week treatment, mice were sacrificed by exsanguination and brains were collected and randomized for biochemical determinations and immunostaining.

Primary neuronal culture

Neuronal cultures from the corticostriatal region of each E18 male and female WT embryo brains were prepared. After dissection, corticostriatal tissue of each embryo was trypsin-digested followed by cell dissociation using a fire-polished Pasteur pipette. Cells were plated on Poly-L-Ornithine-coated dishes in neurobasal medium supplemented with N2 and B27 supplements, 2.0 mM GlutaMAX, 50.0µg/ml penicillin, and 50.0µg/ml streptomycin (ThermoFisher Scientific). Cells were maintained for 12 to 15 days at 37 °C and 5% CO_2 in a humidified incubator before being used for experiments. On the day of the experiment, neuronal primary cultures were incubated with Hank's balanced salt solution (HBSS) for 1h of starvation. After this period, cells were treated with 10 µM CTEP or DMSO (vehicle for CTEP) for 30 min followed by100 nM Human $A\beta_{1-42}$ oligomers (Thermofisher Scientific, 03-111) for 1h or 100 µM (S)-3,5-Dihydroxyphenylglycine (DHPG; Tocris, 0805) for 15 min at 37 °C. $A\beta_{1-42}$ oligomers were prepared in PBS and incubated at 37 °C for 24h as per manufacturer recommendations. Following this treatment, neuronal cultures were lysed with ice-cold lysis buffer and then immunoblotting was performed.

Immunoblotting

All animal experimental protocols were approved by the University of Ottawa Institutional Animal Care Committee and were in accordance with the Canadian Council of Animal Care guidelines. Either a brain hemisphere or neuronal culture well was lysed in ice-cold lysis buffer (50 mM Tris, pH 8.0, 150 mM NaCl, and 1% Triton X-100) containing protease inhibitors cocktail (100µM AEBSF, 2 µM leupeptin, 80 nM aprotinin, 5 µM Bestatin, 1.5 µM E-64 and 1 µM pepstatin A) and phosphatase inhibitors (10 mM NaF and 500 µM Na_3VO_4) and centrifuged twice for 10 min each at 15000 rpm and 4 °C. The supernatant was collected and total protein levels were quantified using Bradford Protein Assay (Biorad). Homogenates were diluted in a mix of lysis buffer and β-mercaptoethanol containing 3x loading buffer and boiled for 10 min at 95°C. Aliquots

containing 30-40 µg total proteins were resolved by electrophoresis on a 7.5% or 10% SDS-polyacrylamide gel (SDS-PAGE) and transferred onto nitrocellulose membranes (Bio-Rad). Blots were blocked in Tris-buffered saline, pH 7.6 containing 0.05% of Tween 20 (TBST) and 5% non-fat dry milk for 2 h at room temperature and then incubated overnight at 4 °C with primary antibodies diluted 1:1000 in TBST containing 2% non-fat dry milk. Immunodetection was performed by incubating with secondary antibodies (anti-rabbit/mouse) diluted 1:5000 in TBST containing 1% of non-fat dry milk for 1 h. Membranes were washed in TBST and then bands were detected and quantified using SuperSignal™ West Pico PLUS Chemiluminescent Substrate (Thermo Scientific).

Sex determination of embryos

DNA was extracted from embryonic tissue by incubation overnight at 55ºC in 500 µl DNA lysis buffer (50 mM Tris (pH 8), 10 mM EDTA, 20 mM NaCl and 0.031% SDS) supplemented with 400 µg/ml Proteinase K. After incubation, lysates were centrifuged at 15000 rpm at 25°C for 10 min and the supernatant was collected. To precipitate DNA, 500 µl isopropanol was added to supernatant. At the end, 50 µl 0.5X Tris-EDTA (Tris HCl 1M, EDTA 0.5M) was added to DNA, heated at 55ºC for 10 min and 2 µl used as template in a 13 µl PCR reaction containing 8.5 µl RNase free water, 1.5 µl 10X buffer, 0.75 µl dNTP, 0.2U Taq DNA polymerase, 1.2 µl MgCl2, and 0.5 µl each primer. Primers were designed flanking an 84 bp deletion of the X-linked Rbm31x gene relative to its Y-linked gametolog Rbm31y (Forward: CACCTTAAGAACAAGCCAATACA; Reverse: GGCTTGTCCTGAAAACATTTGG) (*48*). Reaction were run on ProFlex PCR System (Thermo fisher Scientific) and the thermocycler conditions were 94 °C for 2 min, followed by 30 cycles of 94 °C for 20 s, 60 °C for 20 s and 72 °C for 30 s, with a final elongation at 72 °C for 5 min. PCR reaction were loaded on a 1.5% (w/v) agarose gel containing RedSafe DNA stain (Chembio), electrophoresed in 1X TAE (40 mM Tris acetate, 2 mM EDTA) at 100 V for 25 min and visualized on a Bio-Rad fluorescence system.

Behavioral analysis

Animals were habituated in the testing room for 30 mins prior testing and all behavioral testing was blindly performed during the animal's dark cycle. All behavioral experiments were performed in the Faculty of Medicine Behavior Core Laboratory at the University of Ottawa.

Novel object recognition

Mice were placed in the empty box measuring 45 × 45 × 45 cm for 5 min and 5 mins later, 2 identical objects were placed in the box 5 cm from the edge and 5 cm apart. Mice were returned to the box for 5 min, and allowed to explore, as described previously (*29*). Time spent exploring each object was recorded using a camera fed to a computer in a separate room and analyzed using Noldus Ethovision 10 software. Mice were considered to be exploring an object if their snout was within 1 cm of the object. Each experiment was repeated 24 hours after first exposure with one object replaced with a novel object. Data was interpreted using recognition index which was as follows: time spent exploring the familiar object or the novel object over the total time spent exploring both objects multiplied by 100, and was used to measure recognition memory (TA or TB/ (TA + TB))*100, where T represents time, A represents familiar object and B, novel object.

Open field

Mice were placed in in the corner of an opaque, illuminated (250–300 Lux), white box measuring 45 × 45 × 45 cm and allowed to explore for 10 min, as described previously (*29*). Overhead camera fed to a computer in a separate room monitored the activity and data were analyzed using Noldus Ethovision 10 software. The distance travelled and velocity of each mouse in the open box were determined.

Morris water maze (MWM) and reversal Morris water maze (RMWM)

The Morris water maze test was performed in a white opaque plastic pool (120 cm in diameter), filled with water and maintained at 25°C to prevent hypothermia, as described previously (*23*). A clear escape platform (10 cm diameter) was placed 25 cm from the perimeter, hidden one cm beneath the surface of the water. Visual cues were placed on the walls in the room of the maze as spatial references. Mice were trained for 4 days (four trials per day and 15 mins between trails) to find the submerged platform at a fixed position from a random start point of the 4 equally spaced points around the pool. Each trial lasted either 60 seconds or until the mouse found the platform, and mice remained on the platform for 15 seconds before being removed to their home cage. If the mice failed to find the platform within 60 seconds, they were guided to the platform by the experimenter. Escape latency and swim speed were measured using Ethovision 10 automated video tracking software from Noldus. On day 5, The probe trial (a single trial of 60 seconds) was performed by removing the platform and allowing the mice to swim freely in the pool and recording the time spent in the target quadrant. RMWM task was initiated 24 hours after completion of MWM using the same paradigm as MWM, with 4 days acquisition and probe trial. In the RMWM task, the platform was relocated to a new position.

Determination of Aβ oligomer levels by sandwich ELISA

ELISA was performed as described previously (*23*). Briefly, brains were dissected into right and left hemisphere, with one hemisphere used to analyze oligomeric Aβ levels. Quantification was performed using a sandwich ELISA kit according to manufacturer's instructions, KHB3491 for oligomeric Aβ (Thermo Scientific). Brain homogenates were divided and was centrifuged at 4°C at 100,000 ×g for 1 hour (to measure Aβ oligomer). The supernatant was then diluted with kit buffer 1:10 before carrying out the ELISA, which was performed in triplicate and measured as detailed in the manufacturer's protocol. Protein concentrations were

quantified using the Bradford protein assay. The final Aβ concentrations were determined following normalization to total protein levels.

β-Amyloid, Iba1, Synaptophysin and GFAP immunohistochemistry

Immunostaining was performed as described previously (*23*). Briefly, brains were coronally sectioned through the cortex and hippocampus and staining was performed on 40 μm free-floating sections using a peroxidase-based immunostaining protocol. Sections were incubated overnight in primary antibody for Aβ (1:200), Iba1 (1:100), Synaptophysin (1:100) or GFAP (1:200) at 4°C, washed, incubated in biotinylated antibody (biotinylated horse anti-mouse, 1:400, Vector Elite ABC kit mouse) for 90 mins at 4°C, and then incubated in an avidin biotin enzyme reagent for 90 mins at 4°C (Vector Elite ABC kit mouse, PK-6102, Vector Laboratories). Immunostaining was visualized using a chromogen (Vector SG substrate, Vector Laboratories). Sections were mounted on slides and visualized with a Zeiss AxioObserver epifluorescent microscope with a Zeiss 20× lens, using representative 900 μm^2 areas of cortex and hippocampus. Images were analyzed using the cell counter tool in Image J (NIH, USA).

NeuN immunofluorescence

Coronal brain sections, as described above, were fixed using 4% paraformaldehyde, after which membranes were permeabilized using 0.2% Triton-X-100. Nonspecific binding was blocked using 2.5% normal donkey serum and 1% BSA in PBS, followed by incubation with NeuN primary antibody (1:200) overnight at 4°C. Following a 3x5min wash in PBS sections were incubated in donkey anti-mouse Alexa Fluor 488 (1:400) for 1 hour at room temperature. Sections were mounted on slides and visualized with a Zeiss AxioObserver epifluorescent microscope microscope with a Zeiss 20× lens, using representative 900 μm^2 areas of cortex and hippocampus. Images were analyzed using the cell counter tool in Image J (NIH, USA).

Cell surface biotinylation

Cell surface biotinylation was performed as previously described (*24*). Coronal slices from cortex and hippocampus (350µm) from 2- and 6-month-old mice were prepared using a tissue chopper (McILWAIN tissue chopper, Cavey Laboratory). Slices were transferred to KREBS buffer (127 mM NaCl, 2 mM KCl, 10 mM glucose, 1.2 mM KH_2PO_4, 26 mM NaH_2CO_3, 1 mM $MgSO_4$, 1 mM $CaCl_2$, pH 7.4) continuously gassed with 95%O_2/5%CO_2 for 30 min at 37°C. Slices were then transferred to tubes and biotinylated for 1 hour in 1.5 mg/ml sulfo-NHS-SS-biotin on ice. Slices were then washed and biotinylation was quenched with 100 µM glycine in HBSS for 30 min on ice. Following washes in HBSS, tissue was lysed in RIPA buffer (0.15 M NaCl, 0.05 M Tris–HCl, pH 7.2, 0.05 M EDTA, 1% Nonidet P40, 1% Triton X-100, 0.5% sodium deoxycholate, 0.1% SDS) containing protease inhibitors cocktail (100µM AEBSF, 2 µM leupeptin, 80 nM aprotinin, 5 µM Bestatin, 1.5 µM E-64 and 1 µM pepstatin A). Biotinylated proteins were then pulled down with NeutrAvidin beads using equivalent amounts of proteins for each sample. Biotinylated proteins were separated on SDS-PAGE and immunoblotted with Rabbit polyclonal mGluR5 antibody (1:1000, dilution) as described earlier.

Statistical analysis

Means ± SD are shown for each of independent experiments are shown in the various figure legends. GraphPad Prism software was used to analyze data for statistical significance. Statistical significance was determined by a series of 3 (strain) x 2 (drug treatment) ANOVAs followed by Fisher's LSD comparisons for the significant main effects or interactions.

Figure 1

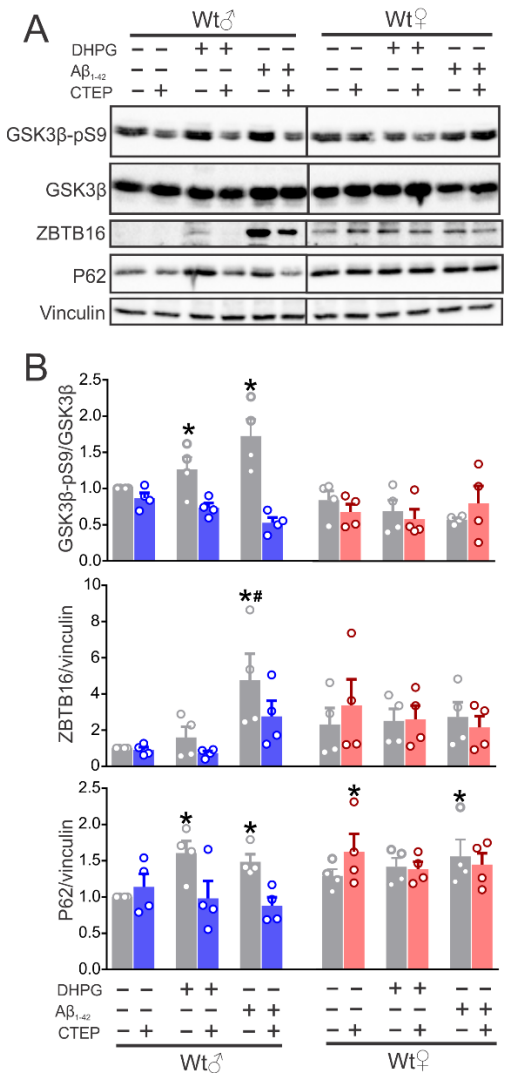

Fig. 1: Activation of mGluR5 modulates GSK3/ATG14ZBTB16 pathway in neuronal cultures from male, but not female, wildtype embryos

Representative western blots **(A)** and quantification of folds change **(B)** in GSK3β-pS9, ZBTB16, and p62 with the corresponding loading controls in primary cultured corticostriatal neurons (14DIV) from male and female wildtype E18 embryos stimulated with either the mGluR group I agonist DHPG (100 μM) or $A\beta_{1\text{-}42}$ oligomers (100 nM) in the absence (DMSO) or presence CTEP (10 μM). GSK3β-pS9 was normalized to total GSK3β, and ZBTB16 and p62 were normalized to vinculin (n=4 for each group). Values represent mean ± SEM and are expressed as a fraction of the untreated male cultures. * P<0.05 versus untreated male cultures. Statistical significance was assessed by two-way ANOVA and Fisher's LSD comparisons.

Figure 2

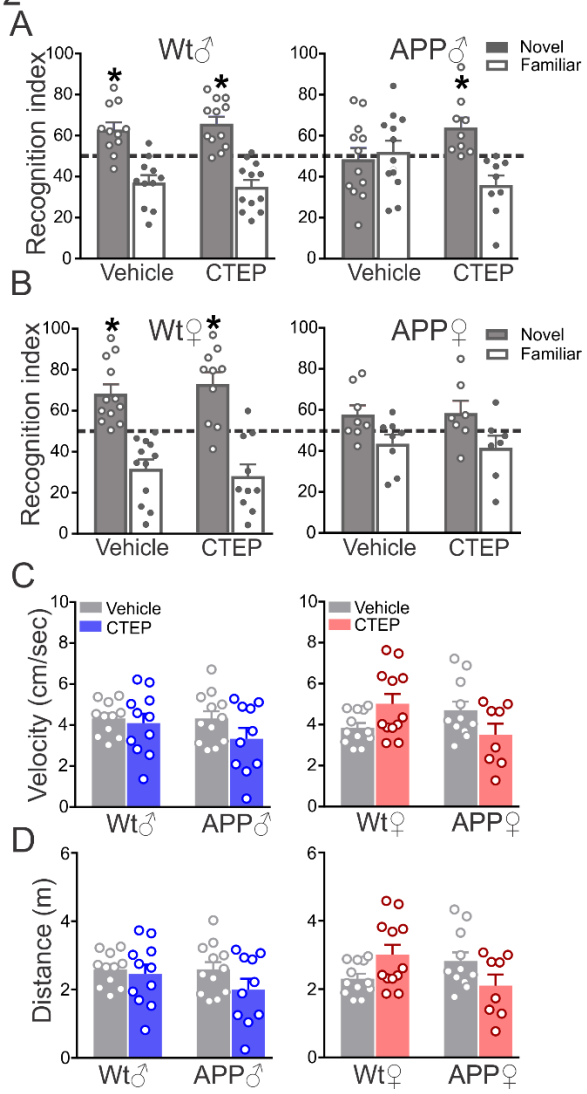

Fig. 2: CTEP improves recognition scores in male, but not female, APPswe/PS1ΔE9 mice.

Mean ± SEM of recognition index, for exploring one novel object versus familiar object in the second day of novel object recognition test following 12-week treatment with either vehicle or CTEP (2mg/kg) in 9-month-old **(A)** male age-matched wild-type (WT) and APPswe/PS1ΔE9 (APP) mice **(B)** female age-matched wild-type (WT) and APPswe/PS1ΔE9 (APP) mice (n=8-11). Mean ± SEM of velocity **(C)** and distance travelled **(D)** following 12-week treatment with either vehicle or CTEP of 9-month-old male and female wild-type (Wt) and APPswe/PS1ΔE9 (APP) mice (n=8-11). Mice were excluded from analysis due to spontaneous death. * P<0.05 versus familiar object. Statistical significance was assessed by two-way ANOVA and Fisher's LSD comparisons.

Figure 3

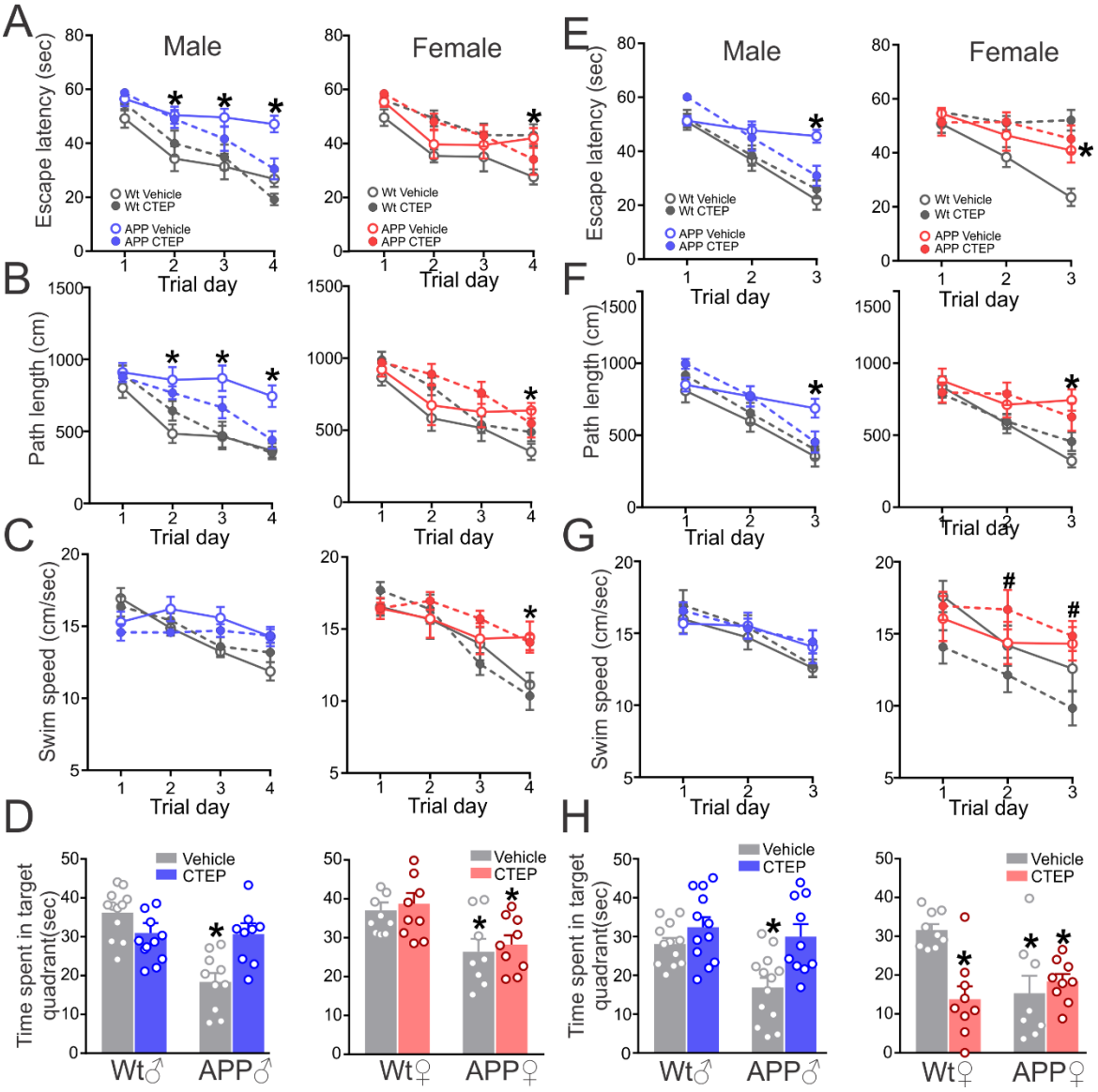

Fig. 3: CTEP improves performance of male, but not female, APPswe/PS1ΔE9 mice in the Morris Water Maze and Morris Water Maze with reversal.

Mean ± SEM of **(A)** escape latency, **(B)** path length and **(C)** swim speed obtained for MWM acquisition phase, and **(D)** time spent in the target quadrant during the probe trial following 12-week treatment with either vehicle or CTEP (2mg/kg) in 9-month-old of male and female wild-type (Wt) and APPswe/PS1ΔE9 (APP) mice. Mean ± SEM of **(E)** escape latency, **(F)** path length and **(G)** swim speed obtained for RMWM acquisition phase, and **(H)** time spent in the target quadrant during the probe trial following 12-week treatment with either vehicle or CTEP in 9-month-old of male and female Wt and APPswe mice (n=8-11). *P<0.05 versus sex-matched vehicle-treated wild-type mice. # P<0.05 versus CTEP-treated wild-type mice. Statistical significance was assessed by two-way ANOVA and Fisher's LSD comparisons. Mice were excluded from analysis due to spontaneous death.

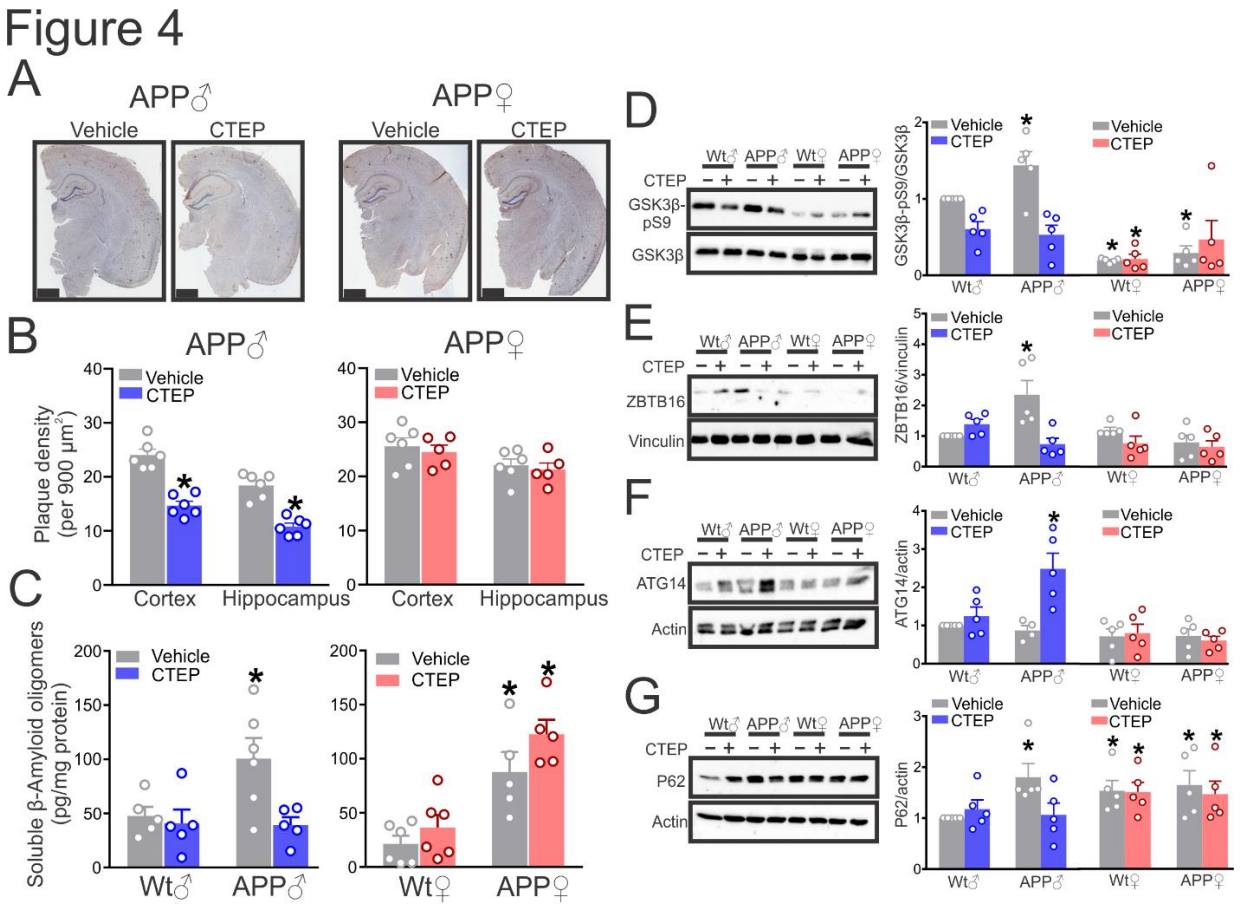

Fig. 4: CTEP reduces Aβ plaques and oligomers and activates autophagy in male, but not female, APPswe/PS1ΔE9 mice.

(A) Representative images of Aβ staining and **(B)** quantification of plaque density in cortical and hippocampal brain slices from 9-month-old male and female APPswe/PS1ΔE9 (APP) mice following treatment with either vehicle or CTEP (2mg/kg) for 12 weeks. Images are representative of 5 independent experiments (scale bar = 1 mm). Data represents mean ± SEM following the quantitation of 5 different 900 μm^2 regions from 6 brain slices of different regions in 5 independent mice for each group. *P<0.05 versus the same region of vehicle-treated same sex APPswe/PS1ΔE9 mice. Statistical significance was assessed by unpaired t test. **(C)** Mean ± SEM of the whole-brain Aβ oligomer concentrations (pg/mg protein) in age-matched 9-month-old male and female wild-type (Wt) and APP after 12-week treatment with either vehicle or CTEP (n=5). *P<0.05 versus vehicle-treated same sex wild-type mice. Statistical significance is assessed by two-way ANOVA and Tukey's multiple comparisons. Representative western blots and quantification of folds change in **(D)** GSK3β-pS9, **(E)** ZBTB16, **(F)** ATG14 and **(G)** p62 with the corresponding loading controls in brain lysates from age matched 9-month-old male and female Wt and APP mice after 12-week treatment with either vehicle or CTEP. GSK3β-pS9 was normalized to total GSK3β, ZBTB16 was normalized to vinculin and ATG14 and p62 was normalized to actin (n=5 for each group). Values represent mean ± SEM and are expressed as a fraction of the vehicle-treated male wild-type value. * P<0.05 versus vehicle-treated male wild-type values. Statistical significance was assessed by two-way ANOVA and Fisher's LSD comparisons.

Figure 5

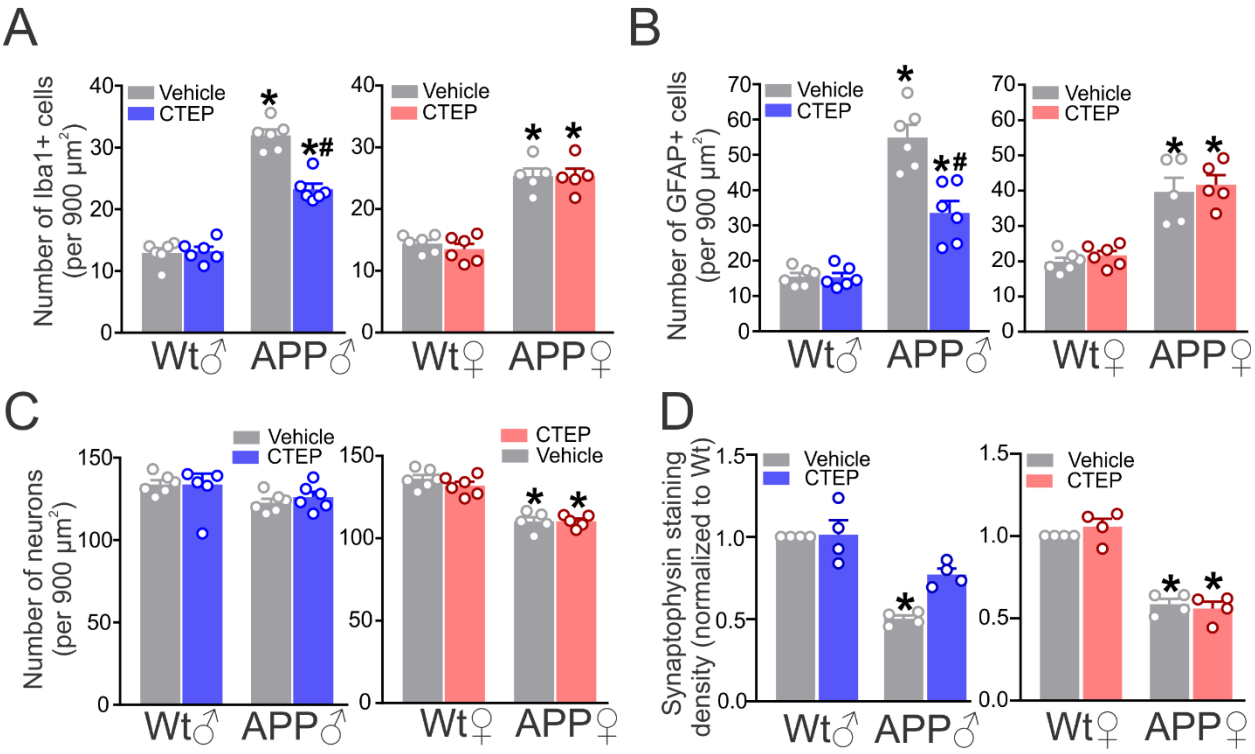

Fig. 5: CTEP reduces neuroglial activation and rescues neuronal and synaptic loss in male, but not female, APPswe/PS1ΔE9 mice.

Quantification of the number of **(A)** Iba1, **(B)** GFAP, **(C)** NeuN positive cells and **(D)** normalized synaptophysin density in 900 μm^2 cortical brain slices from age-matched 9-month-old male and female wild-type (Wt) and APPswe/PS1ΔE9 (APP) mice following 12-week treatment with either vehicle or CTEP (2mg/Kg)**.** Data represents the quantification of 5 different 900 μm^2 regions from 5-6 independent mouse brains for each group. All data is expressed as the Mean ± SEM and synaptophysin density was normalized to sex-matched wild-type values. * P<0.05 versus vehicle-treated same sex Wt value. $^{\#}$P<0.05 versus vehicle-treated male APPswe/PS1ΔE9 value at P < 0.05. Statistical significance was assessed by two-way ANOVA and Fisher's LSD comparisons.

Figure 6

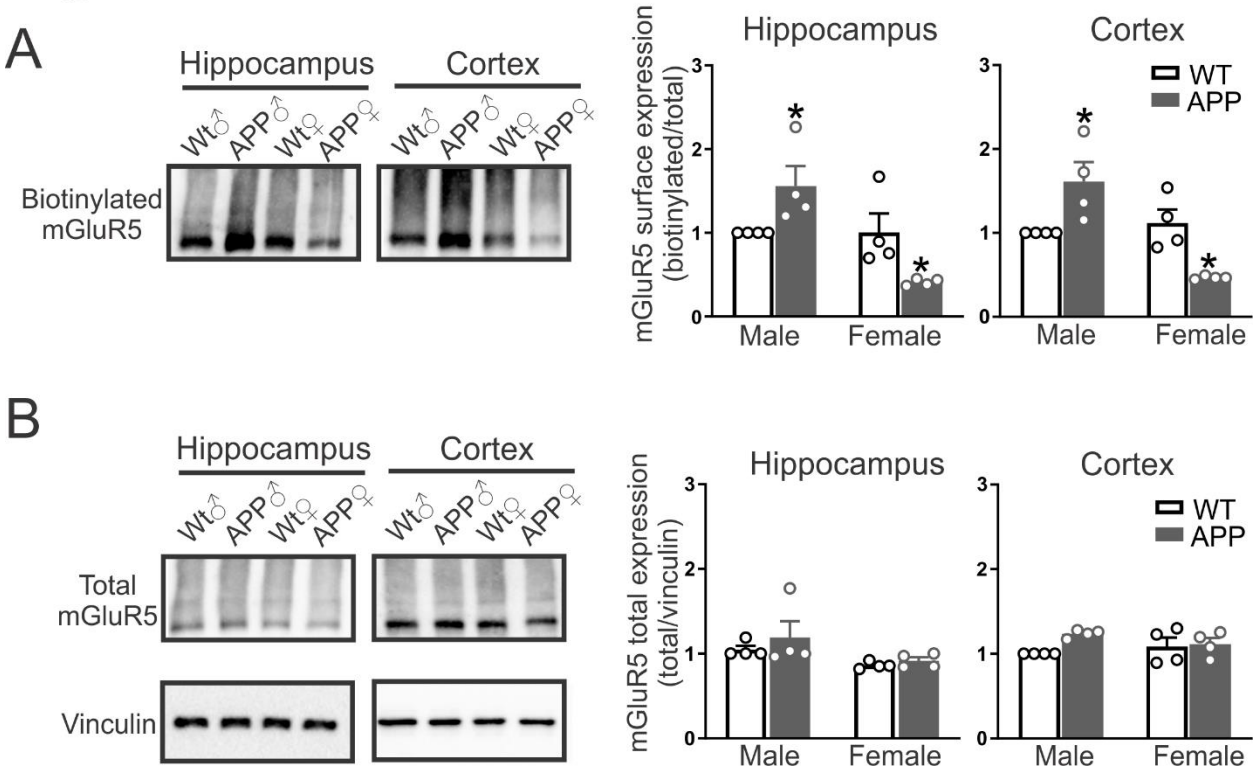

Fig. 6: Differential mGluR5 cell surface expression between male and female APPswe/PS1ΔE9.

Representative western blots and mean ± SEM of mGluR5 cell surface expression **(A)** and total expression **(B)** in cortical and hippocampal brain lysates from age-matched 6-month-old male and female wild-type (Wt) and APPswe/PS1ΔE9 (APP) mice. Values are expressed as a fraction of the male vehicle-treated control for each brain region. Surface expression represents quantification of biotinylated mGluR5 relative to total mGluR5 expression. Total mGluR5 expression was normalized to vinculin (n=4 for each group). * $P<0.05$ versus corresponding male Wt mice. Statistical significance was assessed by two-way ANOVA and Fisher's LSD comparisons.